Summer 2024

Modeling and Control for Precision Robotic Machining

Patrick Bazzoli
Missouri University of Science and Technology

MODELING AND CONTROL FOR PRECISION ROBOTIC MACHINING

by

PATRICK ROBERT THOMAS BAZZOLI

A DISSERTATION

Presented to the Graduate Faculty of the

MISSOURI UNIVERSITY OF SCIENCE AND TECHNOLOGY

In Partial Fulfillment of the Requirements for the Degree

DOCTOR OF PHILOSOPHY

in

MECHANICAL ENGINEERING

2024

Approved by:

Douglas A. Brisow, Advisor
Rober G. Landers
Ming Leu
Akim Adekpedjou
Yun Seong Song

PUBLICATION DISSERTATION OPTION

This dissertation consists of the following two articles, formatted in the style used by the Missouri University of Science and Technology:

Paper I, found on pages 4-28, is intended for submission to *Precision Engineering*.

Paper II, found on pages 29-47, is intended for submission to *IEEE Transactions on Control Systems Technology*.

ABSTRACT

Robots are used in a wide variety of manufacturing applications, but machining applications in which robots can excel are limited by their lower accuracy and stiffness relative to traditional CNC machines. This work is composed of two parts: one to evaluate a robot's accuracy and one to compensate for the vibrations of the robot due to its lower stiffness.

In order to evaluate whether a robot has the necessary accuracy to perform a given machining task, Paper 1 discusses a novel Model Invalidation method. This methodology provides a statistical framework as well as a measurement strategy for determining if a robot is unable to meet a given accuracy requirement. This paper shows through simulation that the Model Invalidation method more accurately evaluates the error in a robot model as compared to other commonly used methods for accuracy identification. Additionally, the Model Invalidation method is shown in implementation on an experimental robot system and results are discussed.

While chatter has always been a widely studied topic in the field of machining, due to their low stiffness, chatter in robots is typically due to deflection of the robot arm itself rather than the deflection of the tool or part. In order to reduce the robot deflections, Paper 2 discusses a structure for designing a vibration suppression controller using an H_∞ framework. Using this framework, control algorithms are designed for an experimental robot machining system to suppress vibrations in both one and two directions, and the results of these controls are discussed.

ACKNOWLEDGMENTS

I would like to thank my advisors Dr Landers and Dr Bristow for guiding me along this journey. Though there were times when we both doubted whether I would reach this point, I know that I could not have made it here without both of you.

I would like to thank my Sensei, Thomas Burden, as well as all of the other friends, students, and teachers that I have met through aikido for helping me discover the type of person that I want to be, giving me an outlet for my stress, providing me with an anchor to Rolla when times got hard.

I would like to thank Le, Michelle, Mitch, Joseph, Eli, and Philip for being behind me until the end, as well as all of my other labmates that have helped me throughout my program. Each and every one of you has left a mark on me and shaped the way that I see and solve problems.

I would like to thank Sean, Will, Jacob, and Zach as well as the rest of the friends that I have made in Rolla for their relentless encouragement to leave this town, and I would like to thank my friend Michael for being with me more years than I can count and showing me that life is full of unexpected twists and turns.

And finally, last but not least, I would like to thank my family for their continued support and for always providing me a home to come back to. I would especially like to thank my niece, Emilia, and my nephew, Benson, for being the two people that wanted me to finish my Ph.D. more than I did.

TABLE OF CONTENTS

Page

SECTION

LIST OF ILLUSTRATIONS

LIST OF TABLES

PAPER I Page

1. INTRODUCTION

In the realm of manufacturing, robots have been traditionally relegated to simple operations, such as pick and place, where the desired locations can be taught and/or touched up by operators; however, there is a growing interest in utilizing robots in more machining processes due to their lower cost and larger workspace-to-footprint ratio as compared to traditional CNC machines. Despite their benefits, robots suffer two major downfalls when compared to their CNC couterparts. Firstly, robots have lower positioning accuracy than traditional CNC machines which can limit the operations that they can perform. And secondly, due to the cantilever-like structure of robots, robots have a lower stiffness than CNC machines, and their stiffness can vary significantly based on their joint configuration. This thesis addresses aspects of both of these issues to improve the machining capabilities of robots.

1.1. ROBOT KINEMATIC MODEL INVALIDATION

Before one can determine the accuracy of a robot, one must first consider what the term “accuracy” means. Often, the term is used without a second thought, but in the simplest sense, accuracy is how well a system (in this case a robot) follows what it is expected to do. In engineering, this expectation is defined by a mathematical model that maps the inputs of a system to its predicted outputs. From this, two important features of accuracy arise. Firstly, accuracy can be thought of as how closely the system matches the model or how closely the model matches the system, but the concept of accuracy only makes sense when there is a specific model that is being evaluated against. The second

important feature of accuracy is that a system is never simply accurate or inaccurate; there is always some measure of accuracy (i.e., one can alway ask how accurate a model is). This means that any arbitrary model of a system is accurate to some level, so the relevant question becomes whether or not a particular model is accurate enough.

Validation is the process of mapping the numerical accuracy value onto a Boolean decision of whether a given model is good enough or not. Typically, validation is performed by acquiring a set of measurements, determining the model's accuracy for each measurement, and evaluating whether these accuracies fall into some level of reasonableness as defined by whoever is taking the measurements. The model is then considered to be "valid" if the reasonableness metric is met. In this approach, there is an implicit assumption that the measurements taken are representative of the model as a whole and that no other measurements would be worse than those taken. While the reasonableness of this assumption varies significantly based on the measurements taken, it is impossible to know with certainty that this assumption holds. On the other hand, if the measurements taken are outside the realm of reasonableness, the model can be considered "invalid" because no additional measurements will ever make the current set of measurements seem more reasonable. This shows that the process of "validation" is ill posed and rather that "invalidation" is the correct approach for assessing model accuracy. In fact, the so-called "validation" method above is actually an invalidation method because the presence of unreasonable measurements (i.e., the model being found invalid) is what would spur the user to take further action.

The first paper in this thesis discusses a rigorous framework for model invalidation as applied to the forward kinematics of a six-axis robot.

1.2. VIBRATION SUPPRESSION FOR CHATTER REDUCTION

While error in kinematic model can encompasses most of the quasi-static errors in the robot, it does not address any of the dynamic errors introduced due to machining. One of the most well-documented sources of dynamic error in machining is chatter. In traditional CNC machines, chatter typically presents itself as regenerative chatter due to deflections in the tool or in the workpiece, but due to the lower stiffness in robots, mode-coupling chatter is typically seen in robots, which is caused by deflections of the robot itself. This chatter typically results in vibrations at the robot's first mode which, due to the low stiffness of robots, occurs at lower frequencies than regenerative chatter and can result in large motions.

In order to fully suppress vibrations on the robot, the controller must be able to eliminate the contributions coming from three different force directions as well as three different moments; however, coupling in the robot's joints these six directions are not completely independent. Because of this, it is desirable to use a control design structure that can generate controllers for multiple axes simultaneously as tuning a single axis at a time can result in subsequent controllers causing previously tuned controllers to no longer meet specifications. One adaptable framework for generating multi-axis control is H_∞ control design.

The second paper in this thesis discusses a formulates an H_∞ control design for performing vibration suppression on machining robots.

PAPER

I. A MODEL INVALIDATION METHOD FOR QUALIFICATION OVER CONTINUOUS SPACES

Patrick Bazzoli, Douglas A. Bristiow, Robert G. Landers

ABSTRACT

When evaluating the accuracy of a system over a continuous space, it is impossible to measure every point, and due to measurement noise, it is impossible to have perfect knowledge of any point that is measured. Furthermore, since the model accuracy and the measurement noise can change over the space, a process that can evaluate model performance over the entire space using a limited number of measurements is necessary. This paper presents a methodology for evaluating the validity of a model while accounting for stochastic errors in the measurement process. The implementation of this method is shown via simulation as well as on an experimental robot system, and the potential utility of this method is discussed.

1. INTRODUCTION

The accuracy of a system is derived by finding the difference between measurements of the system and the desired value or model of the system; however, when taking a finite number of measurements over a continuous space, some data will always be both unknown and unknowable [1] meaning that there is always the possibility

a future measurement being worse than any currently acquired. Because of this, a measured accuracy or "validated" model will not necessarily provide an accurate prediction in all future instances [2]. However, if sufficient data is found to invalidate a model, no additional measurements could possibly make the model valid. Thus, "strictly speaking it is never possible to validate a model, only to invalidate it" [3]. This concept is frequently used during the model construction process to eliminate potential model candidates [4, 5]. Additionally, when performing an invalidation, measurements contain both a bounded error corresponding to the accuracy as well as stochastic error [6] due to measurement noise. Because the validity of a model is determined by the points with the worst model performance [7], stochastic errors in the measurement process make evaluating machine performance sensitive to outliers. Previous work in model invalidation has mitigated this effect by attributing the most possible error to input disturbances and measurement noise during the evaluation process [8], but this method breaks down when using a noise distribution with an infinite support, such as a normal distribution.

One example of the model invalidation problem is qualifying robot accuracy. Due to their high repeatability, robots are typically used in processes where they can be taught specific points such as pick and place operations. In machining operations, it is necessary to ensure that the robot's model, whether derived using the Denavit-Hartenberg convention [9] or an empirical method [10], has sufficient accuracy. Since the stochastic errors in the modeling and calibration process are related to measurement noise [11] as well as machine pose [12], both the bounded accuracy of the model and the stochastic error can change throughout the robot's workspace. This problem requires a methodology

that can balance exploring the robot's workspace with mitigating the noise in the measurement process in order to qualify the true robot accuracy.

The primary contribution of this paper is to provide a statistics-based methodology for determining whether a system is invalid for a given accuracy level. Section 2 of this paper constructs the model invalidation procedure, Section 3 compares model invalidation to common validation methods in simulation, Section 4 discusses an experimental test on a robot, and Section 5 provides summary and conclusions.

2. MODEL INVALIDATION

2.1. PROBLEM STATEMENT

The real world is a continuous space. Part surfaces, machine work volumes, and many other real-world systems and processes all live in this continuous space. When measuring one of these real-world systems using an instrument like a touch probe, an interferometer or even a thermocouple, only a discrete sampling of actual system is taken. Since these systems cannot be measured perfectly, models are used to describe how these systems behave. The question then becomes: how can the discrete measurements of a system be used to determine whether or not the model accurately depicts the true system?

2.2. MODEL INVALIDATION ANALYSIS

In the problem statement above, it is asked whether a model *accurately* depicts the behavior of the physical system. The word accurately is key here because, whether it is a millimeter or a mile, there will always be some error between the model and the

physical system; the magnitude of the error determines the validity of the model. For any point in space, q, the accuracy of the system at that point is defined as the difference between the modeled value, m_a, and the actual value of that system, m_t.

$$e(q) \equiv m_t(q) - m_a(q) \tag{1}$$

While the application of (1) is straightforward in theory, in real-world applications the true value of the system is unknown. Instead, measurements of the system must be used to evaluate the model's error. The difference between the measurements and the system itself is that the measurement process has stochastic error due to positioning repeatability and measurement noise. The positioning repeatability is the ability of the sensor to return to a given q position. In the case of a touch probe, this would be the ability to remeasure a specific point on a part. If the probe does not return to the exact same position, this will add error to the measurement. In contrast, the measurement noise is the derived from the measurement instrument itself. This results in measurements varying even if the instrument stays in a fixed location. Because of these two stochastic errors, the exact value of the true system cannot be determined; however, the magnitude of the error can be bounded with a statistical confidence. This can be done by constructing a hypothesis test using measurements of the error in (1), defined by the random variable X. Assume that X is normally distributed, that is to say

$$X(q) \sim N\left(e(q), \sigma^2(q)\right) \tag{2}$$

where σ is the known standard deviation of measurements at a given position due to the stochastic error in the measurements. For this paper, it is assumed that models for distributions of both the positioning repeatability and measurement noise are known prior

to performing the test. For the model invalidation approach, the null hypothesis, H_0, and the alternate hypothesis, H_1, are

$$\begin{cases} H_0: & e(q) \in [-\eta, \eta] \forall q \\ H_1: & \exists q : e(q) \notin [-\eta, \eta] \end{cases} \tag{3}$$

where η is a pre-defined accuracy level to check the model against. As mentioned above, all models will be accurate to *some* accuracy level, so selecting the correct accuracy to test against is necessary for meaningful results. The accuracy level is entirely process-dependent but can be derived from the part or machine accuracy requirements. The accuracy level can also be selected from previous model performance in order to determine whether the model is still valid. The hypothesis test in (3) is to determine whether or not the true error from (1) is within the selected accuracy level. Using the hypotheses in (3), the rejection criteria for any confidence level, α, is

$$\begin{cases} P(x \mid H_0) < 1-\alpha & \text{Reject } H_0 \\ P(x \mid H_0) \geq 1-\alpha & \text{Fail to Reject } H_0 \end{cases} \tag{4}$$

where **x** is the set of all measurements taken of the error in the system. In order to determine the rejection criteria for the set of all measurements, first consider the rejection probability for a single measurement, $x(q_j)$. The rejection probability is the probability that a new measurement of the error at the same position, q_j, will be closer to $e(q_j)$ than the current measurement is given that $e(q_j)$ is the true error of the system. If $x(q_j)$ is close to $e(q_j)$, the rejection probability is low, and if $x(q_j)$ is far away from $e(q_j)$, the rejection probability is high. Assuming the true position, m_t, is known, the rejection probability, defined as p^*, is

$$Z\left(q_j\right)=\left|\frac{x\left(q_j\right)-e\left(q_j\right)}{\sigma\left(q_j\right)}\right| \qquad (5)$$
$$p^* \equiv \Phi\left(Z\left(q_j\right)\right)-\Phi\left(-Z\left(q_j\right)\right)$$

where Φ is the Cumulative Distribution Function (CDF) of the standard normal distribution defined as

$$\Phi\left(z\right)=\int_{-\infty}^{z}\frac{1}{2\pi}e^{-\frac{x^2}{2}}dx \qquad (6)$$

For further clarity, a graphical representation of p^* is shown in Figure 1.

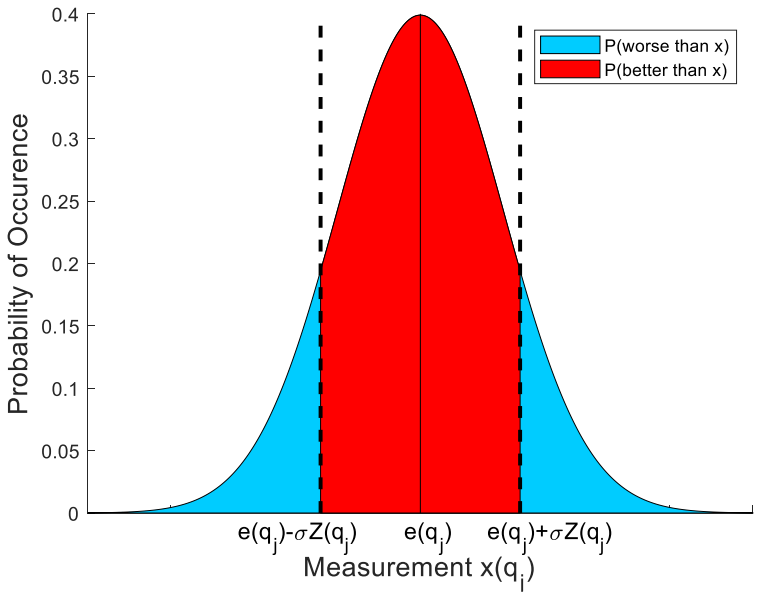

Figure 1: Visual representation where p^* is the area of the red shaded region.

As previously stated, the rejection probability in (5) assumes that only a single measurement is taken at position q_j. If multiple measurements are taken at q_j, the average of the measurements at that position is used instead.

$$\bar{x}\left(q_j\right)=\frac{\sum_{i=1}^{n_j} x_i\left(q_j\right)}{n_j} \tag{7}$$

where x_i is the i^{th} measurement taken at the j^{th} joint command, and n_j is the total number of measurements taken at the j^{th} joint command. From the properties of normal distributions, $\bar{x}\left(q_j\right)$ will still have a mean of $e(q_j)$ but has a standard deviation of

$$\hat{\sigma}\left(q_j\right)=\frac{\sigma\left(q_j\right)}{\sqrt{n_j}} \tag{8}$$

Using the average of the measurements at each location, the p^* value at the j^{th} position is

$$\begin{aligned}\bar{Z}\left(q_j\right)&=\left|\frac{\bar{x}\left(q_j\right)-e\left(q_j\right)}{\hat{\sigma}\left(q_j\right)}\right| \\ p^*\left(e\right)&\equiv\Phi\left(\bar{Z}\left(q_j\right)\right)-\Phi\left(-\bar{Z}\left(q_j\right)\right)\end{aligned} \tag{9}$$

It is important to note that p^* shown in (9) still requires the true value of the system to be known. Because this is not the case with a real set of measurements, consider instead a candidate $\hat{e}\left(q_j\right)$ for $e(q_j)$ such that H_0 in (3) is true. Using this candidate in place of $e(q_j)$ in (9), the p^* value for the candidate can be calculated. The rejection probability of the entire space is

$$P^*\left(\hat{e}\right)=1-\prod_{j=1}^{m}\left(1-p_j^*\left(\hat{e}\right)\right) \tag{10}$$

Using this overall probability, the rejection criterion for the null hypothesis from (4) can be rewritten as

$$\begin{cases} P^*\left(\hat{e}\right) > \alpha & \text{Reject } H_0 \\ P^*\left(\hat{e}\right) \le \alpha & \text{Fail to Reject } H_0 \end{cases} \tag{11}$$

However, since it is unknown whether or not this candidate is equal to the true error function, the rejection of this candidate may or may not yield any information about the true error function. Because of this, the candidate must be selected such that a rejection of the candidate will always result in a rejection of the true error function. One method for doing this is to ensure that the p^* value for the candidate is less than or equal to the p^* value of the true error function at all locations. That is to say

$$p_j^*\left(\hat{e}\right) \le p_j^*, \forall q \in range\left(q\right) \tag{12}$$

By establishing a candidate in this way, the rejection of this candidate will guarantee the rejection of H_0.

Theorem: The acceptance probability in (10) is maximized when the error function candidate is of the form

$$\hat{e}\left(q_j\right) = \begin{cases} -\eta & \bar{x}\left(q_j\right) \in \left(-\infty, -\eta\right) \\ \bar{x}\left(q_j\right) & \bar{x}\left(q_j\right) \in \left[-\eta, \eta\right] \\ \eta & \bar{x}\left(q_j\right) \in \left(\eta, \infty\right) \end{cases} \tag{13}$$

Proof: The $\hat{e}\left(q_j\right)$ from (13) is demonstrated to fulfill the condition in (12) for $\bar{x}\left(q_j\right)$ values following each of the three cases.

Case 1: $\bar{x}\left(q_j\right) \in \left(-\infty, -\eta\right)$

For the null hypothesis in (3) to be true and a new error candidate, $\tilde{e}(q_j)$, to not be equal to $\hat{e}(q_j)$, it must be greater than -η. Since $\hat{e}(q_j)$ is equal to -η for such $\bar{x}(q_j)$, the distance between the measurement and each of the error candidates must satisfy

$$\left|\bar{x}(q_j)-\hat{e}(q_j)\right|<\left|\bar{x}(q_j)-\tilde{e}(q_j)\right| \tag{14}$$

Since the standard deviation is the same for both of these error candidates, this relationship carries to the *Z* values must satisfy

$$\hat{Z}(q_j)=\left|\frac{\bar{x}(q_j)-\hat{e}(q_j)}{\hat{\sigma}(q_j)}\right|<\tilde{Z}(q_j)=\left|\frac{\bar{x}(q_j)-\tilde{e}(q_j)}{\hat{\sigma}(q_j)}\right| \tag{15}$$

Using the *Z* score relationship between the two candidates, the corresponding p^* values for each candidate satisfy

$$p_j^*(\hat{e})=\Phi\left(\hat{Z}(q_j)\right)-\Phi\left(\hat{Z}(q_j)\right)<p_j^*(\tilde{e})=\Phi\left(\tilde{Z}(q_j)\right)-\Phi\left(\tilde{Z}(q_j)\right) \tag{16}$$

This shows that the rejection probability of $\hat{e}(q_j)$ is smaller than that of $\tilde{e}(q_j)$ for measurements in the range (-∞,-η).

Case 2: $\bar{x}(q_j)\in[-\eta,\eta]$

For measurements in this range, the error candidate, $\hat{e}(q_j)$, is set equal to the measurement. This means that for any $\tilde{e}(q_j)$ not equal to the measurement,

$$\left|\bar{x}(q_j)-\hat{e}(q_j)\right|=0<\left|\bar{x}(q_j)-\tilde{e}(q_j)\right| \tag{17}$$

From this point, the logic follows that of Case 1.

Case 3: $\bar{x}(q_j)\in(\eta,\infty)$

This case is a mirror image of the first case meaning that $\hat{e}(q_j)$ is equal to η and $\tilde{e}(q_j)$ must be less than η. From this we obtain the same distance between measurement relation shown by (14). The rest of the proof follows Case 1.

2.3. MODEL INVALIDATION IMPLEMENTATION

The analysis method described above establishes the procedure for calculating the rejection probability from a set of data, but it does not determine how many measurements to take or where to take those measurements when performing invalidation. If an insufficient number of unique positions are taken, the results may not apply to the full range of motion. On the other hand, since a “bad” measurement in one location cannot be averaged out by a “good” measurement at a different location it is unknown whether a location with large error actually falls outside of the accuracy level or if the large error is an artifact of the stochastic measurement process. Because of this, it becomes important to be skeptical of rejection and further investigate locations that yield "bad" measurements. In this way, selecting a measurement location is always a choice between exploring the space and re-interrogating bad measurements. In order to decide where to measure next, consider the sampling strategy shown in Figure 2.

In the sampling strategy shown in Figure 2, if the measurements have a rejection probability below α, the algorithm will continue exploring the space. When considering new measurement locations, optimizing spatial density should be considered so that the results can be applied to the entire machine tool workspace. While there are many ways to select these measurement locations, such as a grid pattern, a pseudo-random pattern, or a quasi-random pattern, this paper uses a quasi-random pattern as it avoids masking

periodic errors while providing low discrepancies as discussed in [13]. If the current set of measurements has a rejection probability above α, the position with the worst rejection probability will be remeasured. When the average measurement from (7) is used to calculate the error term, the spread of the distribution in (9) is reduced as the number of measurements, n_j, increases. This means that as the number of measurements at a given location goes to infinity the distribution goes to a single point, so the value of p_j^* will either be 0 (if the measurement is not in the tolerance range) or 1 (if the measurement is in the tolerance range). Because of this result, if a location is measured an infinite number of times, it will always yield the true response. This means that if the rejection probability is low, the process will infinitely explore the space, and if the rejection probability is high, the process will infinitely measure the worst point. For practical reasons, the process is stopped when either a sufficient spatial density has been reached or a maximum number of measurements has been taken.

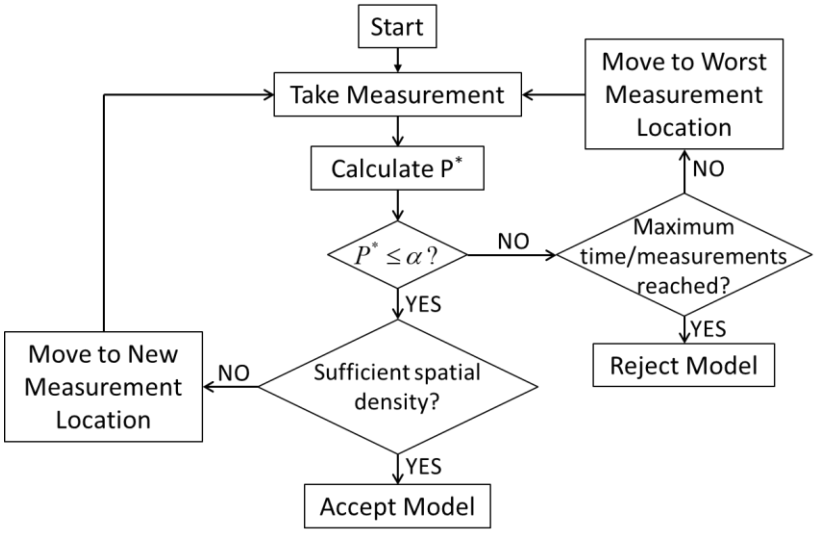

Figure 2: Measurement strategy flowchart.

2.4. APPLICATION TO ROBOT KINEMATIC MODELING

While the method described above focuses on measuring in a one-dimensional space, many systems operate in multi-dimensional spaces. One example to show the extrapolation of the above method to multiple dimensions is the end effector position of a serial kinematic robot. In the field of robotics, the end effector position is described by a forward kinematic model that maps the set of n joint angles, $\mathbf{q}$, to Cartesian space. Both the joint space of the robot and the Cartesian space of the end effector are muli-dimensional continuous spaces. The position vector of the end effector, $T(\mathbf{q})$ is

$$T(\mathbf{q}) = \begin{bmatrix} x_a(\mathbf{q}) \\ y_a(\mathbf{q}) \\ z_a(\mathbf{q}) \end{bmatrix} \tag{18}$$

where x_a, y_a, and z_a are the modeled positions in the x, y, and z directions respectively for a set of joint commands, $\mathbf{q}$. As discussed above, measurements of systems have stochastic error due to positioning repeatability and measurement noise. Since the robot's end effector is positioned through the motion of the individual joints, the positioning repeatability comes from the repeatability of the individual joints. Each joint is assumed to have normally distributed positioning error with zero mean. This means that each joint will nominally go to the commanded position but will actually have some small error. From this assumption, the distribution for the joint positioning error of the i^{th} joint is

$$V_i \sim N\left(0, \sigma_{v,i}^2\right) \tag{19}$$

where $\sigma_{v,i}^2$ is the variance in the positioning of the i^{th} joint. Similarly, the measurement noise, which can be obtained from experimental data or the manufacturer's specifications, is assumed to be normally distributed with zero mean in the x, y, and z directions.

$$\begin{aligned} \Xi_x &\sim N\left(0, \sigma_{\xi,x}^2\right) \\ \Xi_y &\sim N\left(0, \sigma_{\xi,y}^2\right) \\ \Xi_z &\sim N\left(0, \sigma_{\xi,z}^2\right) \end{aligned} \tag{20}$$

where $\sigma_{\xi,x}^2$, $\sigma_{\xi,y}^2$, and $\sigma_{\xi,z}^2$ are the measurement variances in the x, y, and z directions respectively. Since the joint positioning error in (19) acts as a perturbation on the set of joint angles, **q**, and the measurement noise acts as a perturbation on the end effector position, the measured end effector position is

$$T\left(\mathbf{q}+\mathbf{v}, \boldsymbol{\xi}\right) = \begin{bmatrix} x_a\left(\mathbf{q}+\mathbf{v}\right)+\xi_x \\ y_a\left(\mathbf{q}+\mathbf{v}\right)+\xi_y \\ z_a\left(\mathbf{q}+\mathbf{v}\right)+\xi_z \end{bmatrix} \tag{21}$$

where ***v*** is the vector of joint angle errors and ξ_x, ξ_y, and ξ_z are the measurement errors in the x, y, and z directions, respectively. In order to determine the distribution of measurements in each of these three directions, the x, y, and z errors for a given set of joint commands are considered as the output of a dynamic system excited by independent Gaussian variables [14] (i.e., the individual joint repeatabilities and the measurement noise). Because it is assumed that the error from the nominal position is small, the linearization of these functions is used. Consider the linearization of the measurement of the x direction.

$$x\left(\mathbf{q}+\mathbf{v}\right)+\xi_x \approx x_a\left(\mathbf{q}+\hat{\mathbf{v}}\right)\Big|_{\hat{\mathbf{v}}=0} + \frac{\partial x}{\partial \mathbf{v}} + \xi_x \tag{22}$$

Using the linearization as well properties of normal distribution, the approximate distribution of measurements in the x direction is

$$X\left(\mathbf{q}\right) \sim N\left(x\left(\mathbf{q}\right), \sum_{i=1}^{n}\left(\frac{\partial x}{\partial v_i}\right)^2 + \sigma_{\xi,x}^2 \right) \tag{23}$$

The distribution shown above in (23) is the probability distribution of the x position of the end effector; The distributions for the y and z positions are calculated in same manner and are thus excluded for brevity.

When considering the accuracy of the end effector position model, it is useful to consider the magnitude of the error rather than the error in each of the x, y, and z directions separately. Because of this, the single accuracy level, η, that is being checked against is separated into the error bounds for each direction, η_x, η_y, and η_z, using the measurements of the error in each of the three directions, $e_{m,x}$, $e_{m,y}$, and $e_{m,z}$.

$$\begin{aligned} \eta_x &= \frac{e_{x,m}}{\|\mathbf{e}_m\|}\eta \\ \eta_y &= \frac{e_{y,m}}{\|\mathbf{e}_m\|}\eta \\ \eta_z &= \frac{e_{z,m}}{\|\mathbf{e}_m\|}\eta \end{aligned} \tag{24}$$

These directional error bounds are used to generate a candidate error function for each of the three directions using the theorem shown by (13), and the Z-score for each direction is calculated as in (9). The three Z values in the x, y, and z directions are combined into a single test statistic that follows a χ^2 distribution

$$R \equiv \hat{Z}_x^2 + \hat{Z}_y^2 + Z_z^2 \sim \chi^2(3) \tag{25}$$

Using the combined test statistic, R, the p^* value is calculated using the CDF of the χ^2 distribution

$$\begin{aligned} p^*(\hat{e}_x, \hat{e}_y, \hat{e}_z) &= \int_0^R \frac{t^{0.5} e^{-0.5t}}{2^{1.5}\Gamma(1.5)} dt \\ \Gamma(z) &= \int_0^\infty x^{z-1} e^{-x} dx \end{aligned} \tag{26}$$

If multiple three-dimensional measurements are used, the p^* values can be combined as shown by (10) using the same rejection criteria shown in (11).

3. SIMULATION EXAMPLE

3.1. BENCHMARK PROBLEM

In order to evaluate the performance of the model invalidation method described above, the method is compared to common validation methods using a simulation of a single dimensional system. This system is defined to have a sinusoidal error profile of

$$e = \sin\left(2\pi\left(q + 0.1\right)\right) \tag{27}$$

where q is the position over the range [0,1] and e is the error in the system at the corresponding position, q. The error profile for this system is shown below in Figure 3.

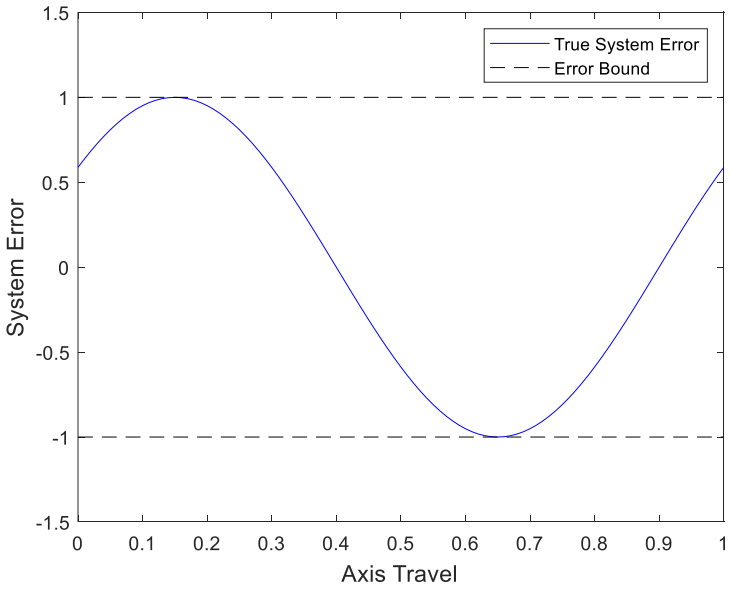

Figure 3: Sinusoidal error profile of simulated system.

This system makes a good benchmark problem for evaluating different validation methods for three reasons. First, it is continuous in q similar to a real system like the surface of a part or a robot's joint space. This means that the system can be sampled infinitely and that it is impossible to the entire workspace. Next, the error in the system is bounded by ±1 and reaches its bound, which means that the true accuracy of the system is known. This allows the evaluation from each method to be compared not just to each other but also to the true value. Finally, the error in the system is non-constant. In real systems, factors such as the limited polynomial order of a model or surface roughness can result in a non-constant error profile. If a sample system with constant error is used, the results may not be generalizable to such problems.

3.2. CATEGORIZATION OF COMMONLY USED METHODS

*Largest Measured Error***:** Typically, when validating a model, the intuitive thing to do is to take a set of measurements and choose your accuracy level equal to the worst measurement [15]. If a sufficient number of measurements are taken, the thought is that worst measurement will correspond to the worst possible performance of the model. This method is the most measurement efficient in terms of exploring the space, but implicitly assumes that the measurement noise is small enough that the largest measurement is indicative of the true performance.

*Outlier Rejection***:** If measurement noise is significant, one method for mitigating the effect of the noise is to remove the measurements identified as outliers caused by noise [16]. This can be done by analyzing the distribution of the measurements and

flagging measurements far from the mean as outliers. While this method requires the same number of measurements as the first method if the model accuracy changes over the space, influential data may be accidentally thrown out.

Mean Error: Another method to reduce the effect of measurement noise is to measure each point multiple times and use the average measurement at each location to determine the accuracy level. The more measurements taken at each location, the more the measurement noise will be reduced. This method does not have the data loss from the outlier rejection method but has reduced measurement efficiency due to the repeated measurement at each point.

3.3. SIMULATION RESULTS

In order to simulate the performance of the three common methods above as well as the model invalidation process, simulated measurements are taken of the error function in (27) at 1000 evenly spaced joint locations over the [0,1] range. These measurements are simulated by adding Gaussian white noise to the error function value at each point using three different noise magnitudes: a low noise with a standard deviation of 0.1, a medium noise with a standard deviation of 0.5, and a high noise with a standard deviation of 1. In the simulation of the outlier rejection method, any data with error magnitude outside of a 95% confidence interval was rejected as outliers, and the multiple measurement method used 10 measurements per point. Since the model invalidation method tests against a fixed accuracy level, the measured accuracy was the largest values that did not result in rejection when a maximum of 100 measurements were taken at each location. The accuracy level from each method is shown below in Table 1.

Table 1 shows that the Largest Error method measures the worst accuracy at each noise level tested. The Outlier Rejection method identifies a lower accuracy than the true model at low noise levels because it throws out relevant data, but at high noise levels, it does not remove enough data to eliminate the effects of measurement noise. The Mean Error method shows consistent improvement over the Largest Error method and measures an accuracy level within 8% of the true accuracy at low noise levels; however, an insufficient number of measurements were taken to mitigate the noise in the higher noise tests. Finally, the Model Invalidation method identifies the best accuracy level in all noise conditions. In order to better understand the accuracy performance of each method, the identified accuracy level of each method is shown for a range of measurement noise between 0 and 1 in Figure 4 below.

Table 1: Identified accuracy of the model from simulated measurements.

Method	**0.1 Noise**	**0.5 Noise**	**1.0 Noise**
Largest Error	1.21	2.49	3.85
Outlier Rejection	0.63	0.99	1.48
Mean Error	1.08	1.53	1.78
Model Invalidaiton	1.01	1.04	1.06

In Figure 4, the Largest Error, Outlier Rejection, and Mean Error methods all show a larger measured accuracy as the measurement noise increases, but the Model Invalidation method adheres more closely to the true accuracy level. The Model Invalidation does show more deviation from the true value at higher noise levels,

indicating that similar to the Mean Error method more measurements are needed to mitigate larger noise.

While Figure 4 shows the accuracy of each method for varying noise levels, these methods require different numbers of measurements and thus different amounts of time to perform. In order to compare each of these methods with respect to time, the accuracy of each method was compared when they were forced to take the same number of measurements. Accuracies of these methods using a noise standard deviation of 0.5 for up to 500 points are shown below in Figure 5.

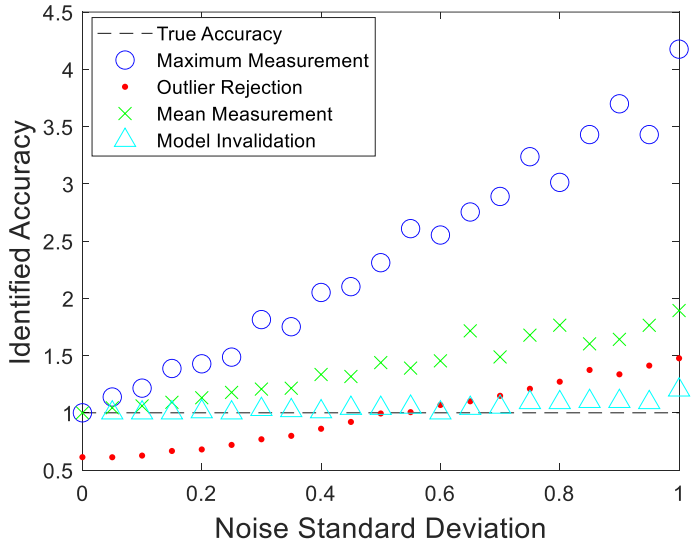

Figure 4: Identified accuracy from simulation at varying noise levels.

In Figure 5 below, the Largest Error method identified the worst accuracy at each of the number of measurements shown. The Mean Error method starts with an accuracy close to 0 due to the order of positions visited and its slow exploration speed and ends with an accuracy of 1.41 after 360 measurements. Both the Model Invalidation method

and the Outlier Rejection method maintain near the true accuracy. From Table 1, this noise level is where the best performance for the Outlier Rejection method.

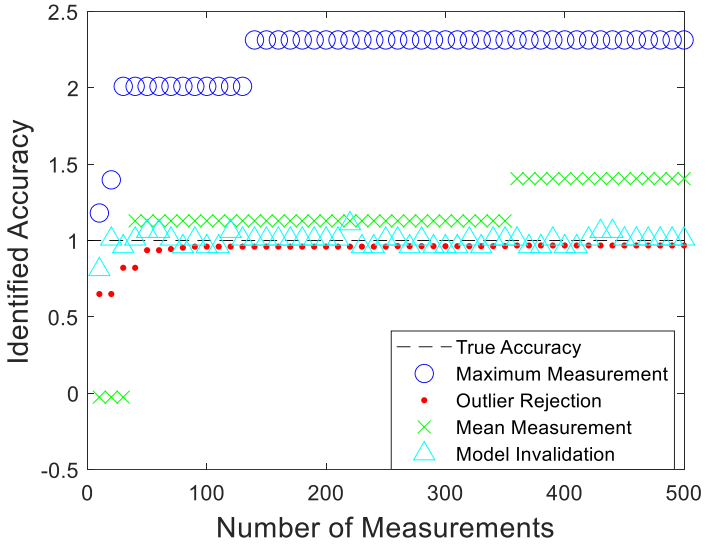

Figure 5: Identified accuracy from simulation for varying number of measurements.

4. EXPERIMENTAL RESULTS

4.1. EXPERIMENTAL SYSTEM

The model invalidation process was performed on the 6 axis robot system shown below in Figure 6.

The robot shown above in Figure 6 is a Motoman MH180 which has a reported repeatability of 0.2 mm. Measurements of the robot's end effector are taken with the API Radian Laser, which has a static measurement accuracy of 5 μm/m, and the API Smart Track Sensor (STS), which has a measurement uncertainty of ±12.5 μm. The robot and the laser tracker are both connected to a Windows 10 computer through ethernet connection and interface through the Robot Operating System (ROS).

Prior to running the invalidation procedure, a model of the robot's position was constructed from 199 quasi random joint configurations using the Volumetric Error Compensation (VEC) method described in [10]. The identification set using this model was found to have a mean error of 0.168 mm and a maximum error of 0.398 mm.

Figure 6: System used in experimental test.

4.2. INVALIDATION TEST

Using the system described above, the model was tested against a 90% confidence level. In order to see if the maximum error in the model was affected by noise, the accuracy level for this test was selected to be 0.375 mm, a value between the measured mean error and the measured maximum error. For this test, 50 additional quasi random joint configurations were selected that were within the same joint range as the model but not used in the modeling process, and a maximum of 10 measurements per joint

configuration were allowed before the model would be rejected. In order to ensure that the measured error corresponded to robot error, the base frame and tool frame errors were minimized after each measurement was taken. The measured robot errors from this test are shown below in Figure 7.

In Figure 7 below, three different measurement locations need to be remeasured as shown by the red x's. Note that the measured error of a given point can change during the measurement process due to the base frame and tool frame updates. This is reason that Point 10 was remeasured despite both measurements being less than the accuracy level in Figure 7. Using the data from this test, the model invalidation process was compared to the Largest Error and Outlier Rejection methods described above. This comparison is shown below in Table 2.

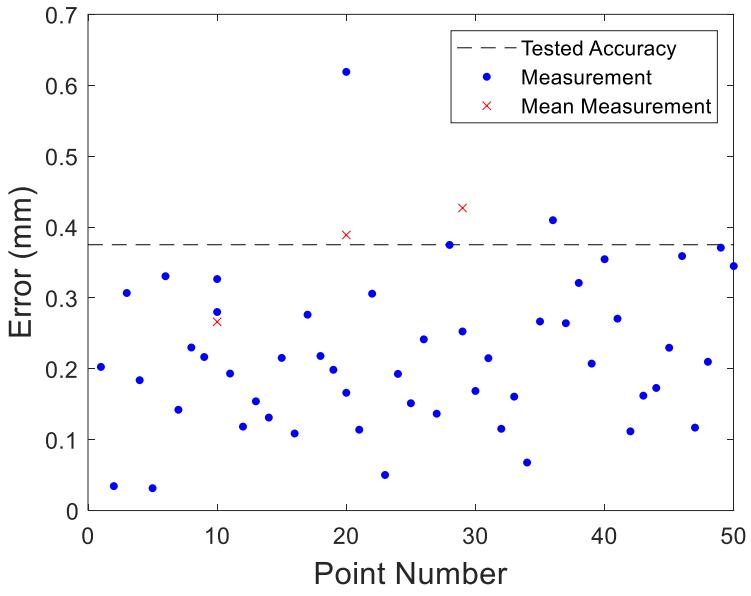

Figure 7: Measured error from invalidation testing on the robot using the final base frame and tool frame fitting.

Table 2: Comparison of model invalidation to other methods.

	Required Measurements	Measured Accuracy (mm)
Largest Error	50	0.619
Outlier Rejection	50	0.41
Model Invalidation	53	0.375

The results shown above in Table 2 mirror the simulation results in Table 1. In terms of measurements required, the Model Invalidation method required three more measurements than the Largest Error or Outlier Rejection methods. Using this metric, the model invalidation method falls between the Largest Error and Mean Error methods. For the measured accuracy level, the model invalidation showed the model to have the least error error of the three methods. While the identified accuracy level could be improved by either testing against a different accuracy level for Model Invalidation method or changing the outlier condition for the Outlier Rejection method, the Largest Error method cannot be improved by taking any more measurements and may even get worse. Overall, the trends in the experimental data line up with the trends found in simulation.

5. SUMMARY AND CONCLUSIONS

By using models of sensor positioning repeatability and the measurement noise distributions, a metric was constructed that is capable of determining if the model of the system is invalid to a given accuracy level, and a methodology was described to implement that metric. This method was then implemented through a simulation on a one-dimensional system as well as experimentally on a six-axis robot. In the simulation,

model invalidation better identified the accuracy of the model than the other methods tested, being within 6% of the true value in a high noise setting and showed improved measurement efficiency over a single measurement and uniform remeasurement approach. Similar results were found in the experimental data, where model invalidation required only 3 additional measurements and evaluated the model as having higher performance than the other methods tested. Overall, the model invalidation method is a rigorous process for evaluating model performance, especially in noisy systems.

ACKNOWLEDGEMENT

This work was supported by the National Science Foundation (CMMI 1335340) and the GAANN Fellowship. A special thanks goes to the Center of Aerospace Manufacturing Technology for the use of their facilities and equipment.

REFERENCES

[1] Beck, M., Ravetz, J., Mulkey, L., and Barnwell, T., 1997. “On the problem of model validation for predictive exposure assessments”. Stochastic Hydrology and Hydraulics, 11(3), pp. 229–254.

[2] Hassanizadeh, S., and Carrera, J., 1992. Validation of geo-hydrological models. 1.

[3] Smith, R. S., and Doyle, J. C., 1992. “Model validation: A connection between robust control and identification”. IEEE Transactions on automatic control, 37(7), pp. 942–952.

[4] Sokolov, V. F., 2003. “Robust control in 1-formulation: Model validation and perturbation weight estimation”. Automation and Remote Control, 64(11), pp. 1769–1781.

[5] Roberts, M. A., August, E., Hamadeh, A., Maini, P. K., McSharry, P. E., Armitage, J. P., and Papachristodoulou, A., 2009. “A model invalidation-based approach for elucidating biological signalling pathways, applied to the chemotaxis pathway in r. sphaeroides”. BMC Systems Biology, 3(1), p. 105.

[6] Newlin, M. P., and Smith, R., 1991. “Model validation and a generalization of mu”. In [1991] Proceedings of the 30th IEEE Conference on Decision and Control, IEEE, pp. 1257–1258.

[7] Anderson, J., and Papachristodoulou, A., 2009. “On validation and invalidation of biological models”. BMC bioinformatics, 10(1), p. 132.

[8] Newlin, M. P., and Smith, R. S., 1998. “A generalization of the structured singular value and its application to model validation”. IEEE Transactions on Automatic Control, 43(7), pp. 901–907.

[9] Hartenberg, R. S., and Denavit, J., 1955. “A kinematic notation for lower pair mechanisms based on matrices”. Journal of applied mechanics, 77(2), pp. 215–221.

[10] Ma, L., Bazzoli, P., Sammons, P. M., Landers, R. G., and Bristow, D. A., 2018. “Modeling and calibration of high-order joint-dependent kinematic errors for industrial robots”. Robotics and Computer-Integrated Manufacturing, 50, pp. 153–167.

[11] Patel, A. J., and Ehmann, K. F., 2000. “Calibration of a hexapod machine tool using a redundant leg”. International Journal of Machine Tools and Manufacture, 40(4), pp. 489–512.

[12] Nahvi, A., and Hollerbach, J. M., 1996. “The noise amplification index for optimal pose selection in robot calibration”. In Proceedings of IEEE International Conference on Robotics and Automation, Vol. 1, IEEE, pp. 647–654.

[13] Creamer, J., Sammons, P. M., Bristow, D. A., Landers, R. G., Freeman, P. L., and Easley, S. J., 2017. “Table-based volumetric error compensation of large five-axis machine tools”. Journal of Manufacturing Science and Engineering, 139(2), p. 021011.

[14] Kalman, R. E., 1960. “A new approach to linear filtering and prediction problems”. Journal of basic Engineering, 82(1), pp. 35–45.

[15] Jung, J.-H., Choi, J.-P., and Lee, S.-J., 2006. “Machining accuracy enhancement by compensating for volumetric errors of a machine tool and on-machine measurement”. Journal of Materials Processing Technology, 174(1-3), pp. 56–66.

[16] Betke, M., and Gurvits, L., 1997. “Mobile robot localization using landmarks”. IEEE transactions on robotics and automation, 13(2), pp. 251–263

II. H_∞ CONTROL FOR VIBRATION SUPPRESSION IN ROBOTIC MACHINING

Patrick Bazzoli, Douglas A. Bristow, Robert G. Landers

Department of Mechanical and Aerospace Engineering, Missouri University of Science and Technology, Rolla, MO 65409

ABSTRACT

Chatter is a well-studied machining phenomenon that is known to adversely affect part quality. In robotic machining processes, the problem of chatter is amplified relative to standard CNC machining due to the reduced stiffness in the mechanical structures of robots. One potential way to reduce chatter is through active vibration suppression. This paper discusses the design and implementation of a reaction force vibration isolation control algorithm using an H_∞ control structure on a robotic machining setup.

1. INTRODUCTION

In the world of machining, chatter is a heavily studied phenomenon. Typically, in the case of CNC machines regenerative chatter is the primary focus due to their high rigidity; however, in robots, which have much lower stiffnesses, mode coupling chatter tends to be the dominating effect [1]. Some researchers have tried to mitigate these vibrations by modeling the stiffness of the robot in various configurations and performing their machining in the stiffest regions of the workspace [2,3]. While this has the benefit of not requiring additional equipment, it limits the usable workspace of the robot, which

is one of its key benefits over traditional CNC machining. Other research groups have tried to reduce chatter by passively damping the vibrations on the robot [4]; however, such methods require physical changes to the system if robot's resonant mode changes. Because of this, a method of active vibration suppression is useful for robotic machining.

Active vibration suppression has been used in a variety of fields such as active suspensions for cars [5,6] vibration isolation tables [7]. In both of these cases, the acceleration of the system (e.g., the car or the tabletop) is measured and a counteracting force is applied to the ground to cancel the acceleration. Some groups have implemented similar vibration reduction strategies on robots [8], but this restricts the position and orientation with which a robot can machine. One alternative to this approach involves using the motion of the robot itself [9]. Due to the bandwidth required for this, a low-level integration is necessary with the robot's motion controller. Another form of vibration suppression, which is commonly used is in free standing structures, is proof mass vibration suppression [10]. In this case, a proof mass is oscillated back and forth relative to the system, and the force of the mass moving suppresses vibrations. This allows for arbitrary robot configurations without requiring direct integration with the robot's controller.

The proof mass vibration suppression problem is a multivariate problem. Even when only performing vibration suppression on a single axis, it is important to control not only the robot's vibrations but also the mass's position to prevent drifting in the center of the oscillation range that can lead to control saturation. This results in an underactuated system since only one control value determines both outputs. While a variety of control techniques have been used on underactuated systems [11,12], the H_∞ framework [13],

which has been used in the design of vibration suppression for buildings [14], can automatically handle the coupling between variables. This structure also has the added benefit of being easily expandable to additional axes of vibration suppression.

The primary contribution of this paper is to provide a framework for designing a vibration suppression control using an H_∞ structure. Section 2 of this paper discusses the reaction force vibration suppression modeling as well as the H_∞ control framework used in the problem, Section 3 describes the controller and results on a experiment robot system, and finally Section 4 covers conclusions of the results.

2. PROBLEM FORMULATION

2.1. REACTION FORCE MODELING

The robot vibration isolation system can be modeled as two mass-spring-damper systems connected in series. The robot itself is modeled as a large mass, *M*, with a stiffness, *K*, and damping, *B*, acted upon by an external force, *d*. The reaction mass, *m*, is assumed to be connected to the robot with a damping of *b* and a small stiffness, *k*. A voice coil actuator oscillates the reaction mass relative to the robot, which provides a control force, *u*, on both the robot and the reaction mass. A schematic of this system is shown below in Figure 1.

Summing the forces on the large mass, *M*, in the x_1 direction results in

$$d - u + b\left(\dot{x}_2 - \dot{x}_1\right) + k\left(x_2 - x_1\right) - M\ddot{x}_1 - B\dot{x}_1 - Kx_1 = 0 \tag{1}$$

Taking the Laplace transform of (1) and collecting x_1 and x_2 terms results in

$$D(s) - U(s) + (bs + k)X_2(s) - \left(Ms^2 + (B + b)s + (K + k)\right)X_1(s) = 0 \tag{2}$$

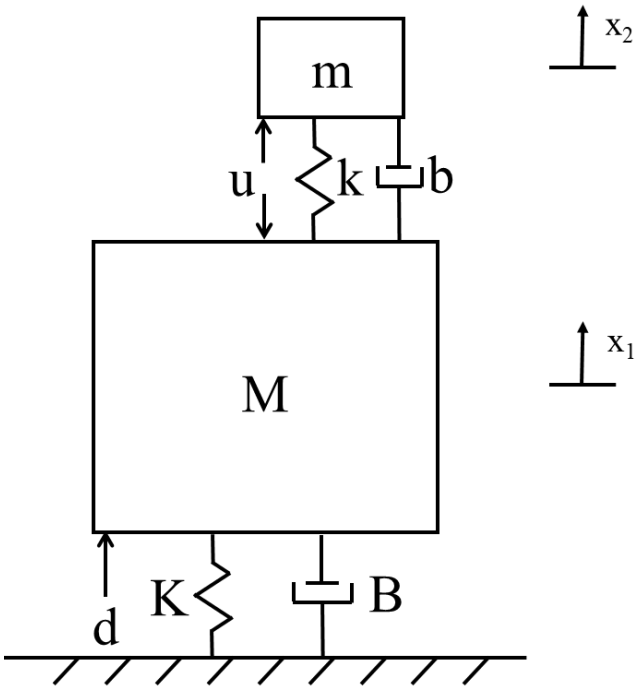

Figure 1: Free body diagram of raction force vibration isolation system.

By moving the x_1 terms to the other side and dividing by the multiplier the equation becomes a function of *d*, *u*, and x_2.

$$X_1(s) = \frac{1}{Ms^2 + (B+b)s + (K+k)}\left[D(s) - U(s) + (bs+k)X_2(s)\right] \tag{3}$$

In order to eliminate the x_2 terms in (3), the forces were summed about the small mass, *m*, in the x_2 direction.

$$u - m\ddot{x}_2 + b(\dot{x}_1 - \dot{x}_2) + k(x_1 - x_2) = 0 \tag{4}$$

Taking the Laplace transform and collecting x_1 and x_2 terms results in

$$U(s) + (bs+k)X_1(s) - (ms^2 + bs + k)X_2(s) = 0 \tag{5}$$

Solving for x_2, (5) becomes

$$X_2(s) = \frac{1}{ms^2 + bs + k} U(s) + \frac{bs + k}{ms^2 + bs + k} X_1(s) \tag{6}$$

Plugging (6) into (3) to eliminate x_2 becomes

$$X_1(s) = \frac{D(s) - U(s) + (bs + k)\left[\frac{1}{ms^2 + bs + k} U(s) + \frac{bs + k}{ms^2 + bs + k} X_1(s)\right]}{Ms^2 + (B + b)s + (K + k)} \tag{7}$$

Collecting the x_1 terms and the u terms together results in

$$\left[Ms^2 + (B + b)s + (K + k) - \frac{b^2 s^2 + 2kbs + k^2}{ms^2 + bs + k}\right] X_1(s) = D(s) - \frac{ms^2}{ms^2 + bs + k} U(s) \tag{8}$$

When reducing the left side, the equation in (8) becomes

$$\begin{aligned} L(s) X_1(s) &= D(s) - \frac{ms^2}{ms^2 + bs + k} U(s), \\ L(s) &= \left[\frac{s^4 + \left(\frac{B + b}{M} + \frac{b}{m}\right)s^3 + \left(\frac{(K + k)}{M} + \frac{k}{m} + \frac{Bb}{Mm}\right)s^2 + \frac{Bk + Kb}{Mm} s + \frac{Kk}{Mm}}{\frac{1}{Mm}(ms^2 + bs + k)}\right] \end{aligned} \tag{9}$$

Dividing by the left-hand side results in x_1 as a function of d and u.

$$\begin{aligned} X_1(s) = &\left(\frac{\frac{1}{M} s^2 + \frac{b}{mM} s + \frac{k}{mM}}{Den(s)}\right) D(s) \\ &- \left(\frac{\frac{1}{M} s^2}{Den(s)}\right) U(s) \\ Den(s) = &\, s^4 + \left(\frac{B + b}{M} + \frac{b}{m}\right)s^3 + \left(\frac{(K + k)}{M} + \frac{k}{m} + \frac{Bb}{Mm}\right)s^2 + \frac{Bk + Kb}{Mm} s + \frac{Kk}{Mm} \end{aligned} \tag{10}$$

Similarly, the position of the reaction mass relative to the robot, $X_2(s)$-$X_1(s)$, can also be found by combining (3) and (6). The resulting transfer functions is

$$X_2(s) - X_1(s) = \left(\frac{-\frac{1}{M} s^2}{Den(s)} \right) D(s) + \left(\frac{\frac{m+M}{mM} s^2 + \frac{B}{mM} s + \frac{K}{mM}}{Den(s)} \right) U(s) \tag{11}$$

By combining the transfer functions based on control input in (10) and (11), the plant model of the system relative to the control input is the 2x1 vector

$$G_u = \begin{bmatrix} \frac{\ddot{X}_1(s)}{U(s)} \\ \frac{X_2(s) - X_1(s)}{U(s)} \end{bmatrix} \tag{12}$$

Similarly, the effect of disturbances on the robot's acceleration and the reaction mass's position is described by the 2x1 vector

$$G_d = \begin{bmatrix} \frac{\ddot{X}_1(s)}{D(s)} \\ \frac{X_2(s) - X_1(s)}{D(s)} \end{bmatrix} \tag{13}$$

The plant models shown in (12) and (13) are used for the reaction force control design.

2.2. H_∞ CONTROL DESIGN STRUCTURE

As shown above in Figure 1, the reaction force vibration isolation model consists of two outputs, the robot's position/acceleration and the reaction mass's position, but only a single control force. Due to the innate coupling of this problem as well as a desire to make the control design expandable to additional axes of vibration isolation, a flexible architecture like H_∞ design is desirable for this problem. For H_∞ control design, a modified plant model is used that takes in exogenous inputs and generates exogenous outputs, which correspond to the signals being minimized. This modified plant includes not only the true plant model of the system, but also weighting functions for each of the exogenous outputs. The H_∞ plant model for the single-axis vibration isolation is shown below in Figure 2.

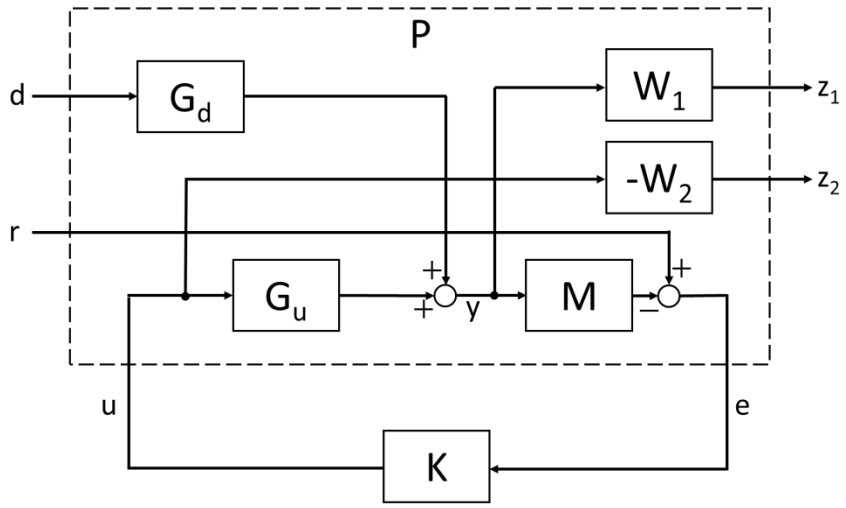

Figure 2: H_∞ control system framework.

In Figure 2 above, the exogenous inputs are the disturbance force, *d*, and the 2x1 reference vector for the robot acceleration and mass position, and the exogenous outputs

are z_1, which is a 2x1 vector that consists of the two outputs, robot acceleration and mass position, and z_2, which is the control signal. G_d represents the transfer function from the disturbance force to the outputs, as shown in (13), G_u represents the transfer function from the control force to the outputs, as shown in (12), and M is used to describe any additional sensor dynamics. Finally, the weighting function W_1 is a 2x1 vector that weights each of the output signals in the H_∞ design, and the weighting function W_2 weights the control signal.

3. EXPERIMENTAL RESULTS

3.1. EXPERIMENTAL SETUP

The vibration isolation described above was tested on the experimental robot system shown below in Figure 3.

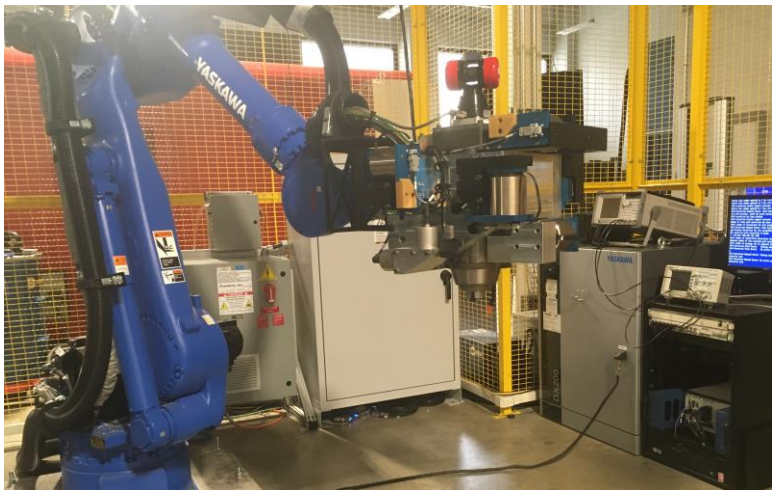

Figure 3: Robot reaction force vibration isolation system.

In Figure 3 above, a Yaskawa Motoman MH180 robot is equipped with a custom-built vibration isolation end effector consisting of 6 H2W Technologies voice coil positioning stages and 6 PCB Piezotronics ICP accelerometers, which are arranged to allow a full 6 DoF vibration isolation. The control is performed in Labview using a National Instruments PXI system, which reads the 6 accelerometers as well as the voice coils' encoder signals and provides a control voltage to an Advanced Motion Controls AxCent servo drive which in turn drives the actuators.

3.2. H_∞ CONTROL DESIGN

Using the experimental system above, a vibration suppression control algorithm was generated using models of the system and selected weighting functions. As described above in the H_∞ control design structure, three different weighting functions are used. For the control signal, a high penalty is place at low frequencies because control input results in large actuator motions at low frequencies but smaller motions at higher frequencies. The actuator position also has a penalty at low frequencies in order to reduce steady state error and keep the actuators near the center of their range. Finally, the acceleration weight was selected to match the roll off of G_{d1} to encourage the minimization to prioritize the acceleration at the robot's mode. These three weighting functions are shown below in Figure 4.

Using the weighting functions shown in Figure 4, an H_∞ controller was generated using the structure from Figure 2. The frequency response for both the acceleration control portion as well as the actuator mass position control portion are shown below in Figure 5.

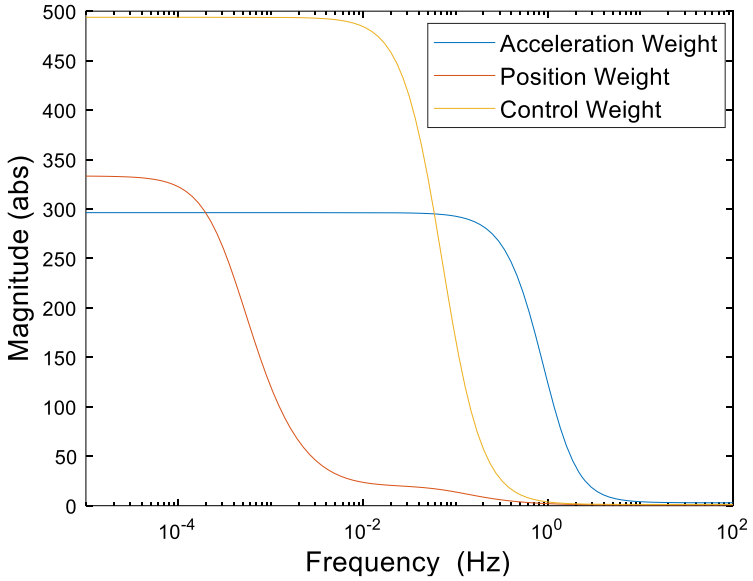

Figure 4: H_∞ design weights.

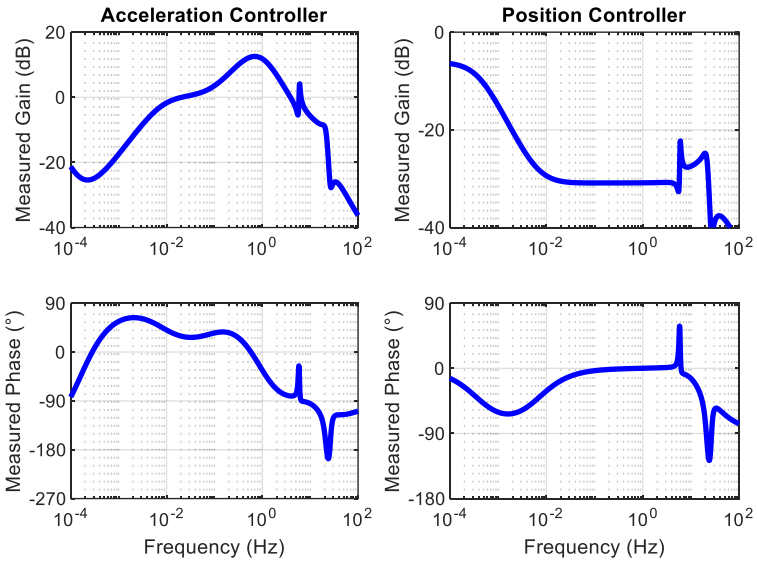

Figure 5: Designed H_∞ controllers.

In Figure 5 above, the acceleration controller shows low gains at low frequencies to eliminate the low frequency noise in the accelerometers and acts like a lowpass filter at

higher frequencies to attenuate high frequency noise, thus only providing control action near the desired mode of the robot. The position controller acts like a PI controller with higher gains at low frequencies. Additionally, both portions of the controller show a spike in both magnitude and phase at the modeled robot mode of 6 Hz. This allows the controller to provide additional performance right at the robot's resonant frequency. In a normal rigid and unchanging system, this additional control authority would be a boon; however, in a robot system where the mode changes based on the robot's pose, the antiresonance that proceeds the gain spike can cause a decrease in performance. In order to increase the control design's robustness to the robot's mode shifting, this resonance/antiresonance pair was manually removed from the H_∞ controller. The frequency responses for the modified H_∞ controller design is shown below in Figure 6.

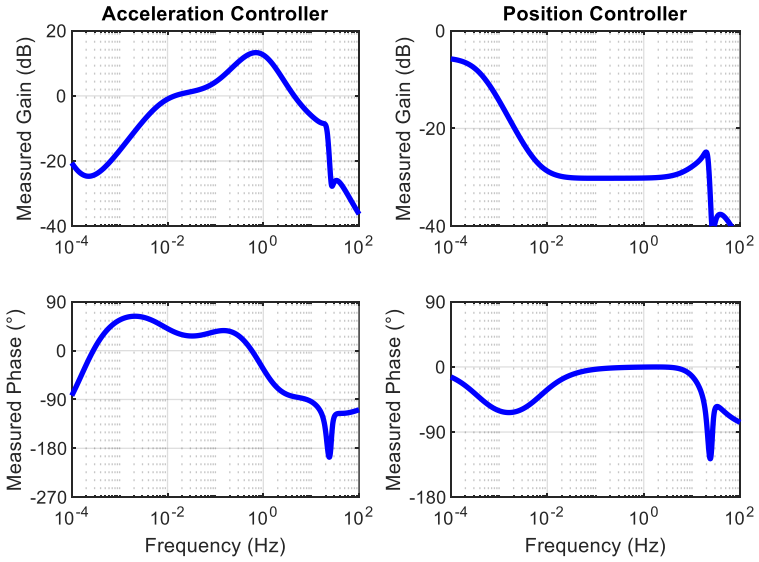

Figure 6: Modified H_∞ controllers.

The modified H_∞ control design shown above in Figure 6 has the same overall shape as the original controller in Figure 5 except without the resonance/antiresonance pair around 6 Hz. This effect of removing these dynamics can be seen in the robot's modeled sensitivity to vibrations with each of these controllers, as shown below in Figure 7.

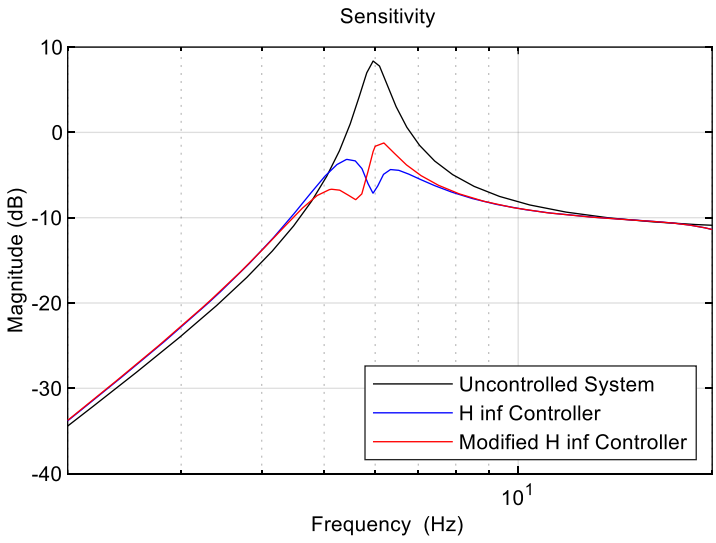

Figure 7: Modeled system sensitivity to disturbances.

In Figure 7 above, the two controllers have similar behaviors except for near the resonance. The original H_∞ controller has a greater reduction right at the resonance location and at slightly higher frequencies, while the modified H_∞ controller has greater reductions below the resonance. Through experimentation, it was seen that the robot's actual resonance tends to shift to the left of the model in Figure 7, so the modified controller is a better choice for this application.

3.3. SINGLE-AXIS IMPLEMENTATION TEST

In order to test the modified H_∞ controller's performance on the actual system, two different tests were performed with the robot in the same configuration. The first test determined the robot's open-loop performance by using a digital signal analyzer. The digital signal analyzer measured the robot's frequency response at the current configuration by sending a range of sinusoidal voltage inputs to one of the system's voice coil actuators to provide a disturbance to the system and measuring the response of one of the accelerometers. The closed-loop test was performed the same way except the accelerometer signal was also fed into the modified H_∞ controller which then actuated a second voice coil to dampen out the disturbance. Figure 8 below shows the interconnection of each of the components for the uncontrolled test (in blue) and the controlled test (in red).

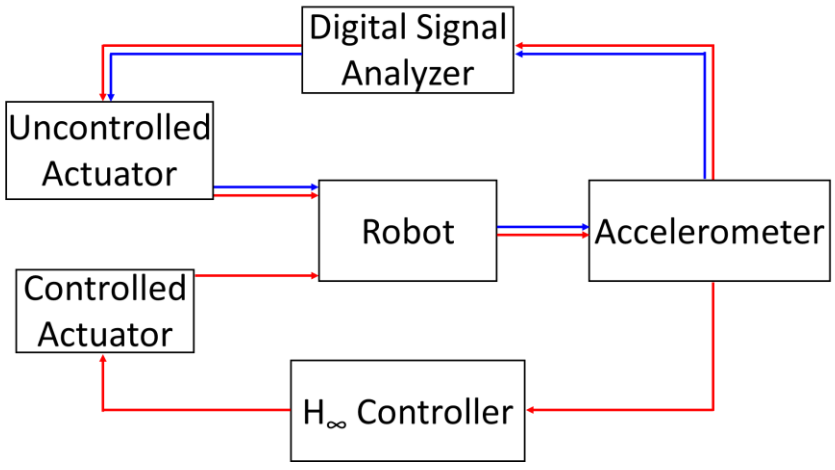

Figure 8: Single-axis control test block diagram.

The magnitude from each of the frequency responses for the two tests are shown below in Figure 9.

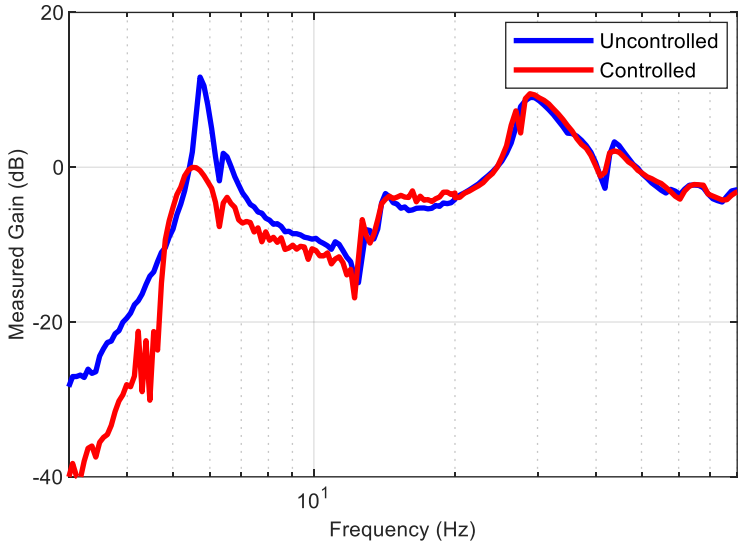

Figure 9: Measured uncontrolled and controlled acceleration sensitivity.

Figure 9 above shows that the modified H_∞ controller was able to successfully reduce the vibrations at the robot's 5.72 Hz mode by 75.2% without amplifying any of the higher frequency vibrations.

3.4. TWO-AXIS VIBRATION TEST

In order to test the H_∞ control design in a situation more analogous to machining, an eccentric mass was put into the robot's spindle as shown below in Figure 10 and was rotated to induce a disturbance on the system.

Figure 10: Setup for eccentric mass experiment.

Because the eccentric mass creates vibrations in both robot's tangential direction and its axial direction, a second H_∞ controller was designed using the same process above and applied to one of the actuators in the axial direction. The resulting H_∞ controller is shown below in Figure 11.

With the eccentric mass attached to the robot, the spindle was rotated at 20 different frequencies between 2 and 20 Hz and accelerometer measurements were taken in the robot's axial and tangential directions. For each frequency, the Fourier transform was taken of the acceleration data, and the magnitude at the excitation frequency was recorded. Figure 12 below shows the resulting magnitudes for both the uncontrolled test

as well as the test when the controllers in Figure 6 and Figure 11 are applied to the tangential and axial directions, respectively.

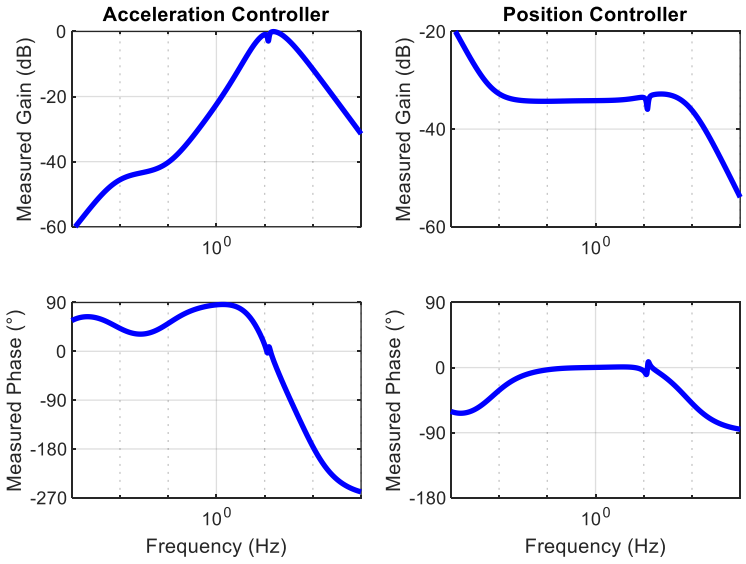

Figure 11: Modified H_∞ controller for robot's axial direction.

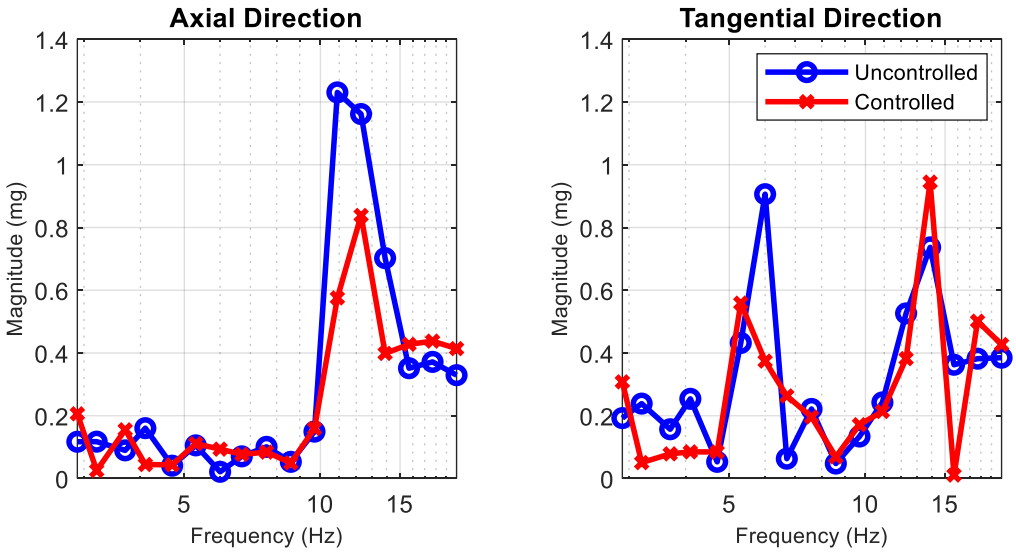

Figure 12: Measured acceleration in uncontrolled and controlled eccentric mass test.

Figure 12 above shows that the axial controller was able to successfully reduce the robot's mode at 12.3 Hz by 27.8%, and the tangential controller reduced the robot's mode at 6.0 Hz by 58.7%. While the tangential response does show an increase at 13.9 Hz, this is likely due to the decreased gain of the tangential controller at 14 Hz (as compared to its designed frequency of 6 Hz) combined with induced coupling and/or rotations from the activity of the axial controller. It is expected that this performance would be improved if both directions were combined into the same H_∞ minimization.

4. CONCLUSION

In this paper, a dynamic model for the single-axis reaction force vibration isolation problem was presented as well as an H_∞ architecture for this problem. Using this architecture, an H_∞ controller was designed and implemented on an experimental robotic machining system. In the single-axis experiment, the controller caused a 75.2% reduction in vibrations at the robot's resonant frequency of 5.72 Hz. In the 2D test where two single-axis controllers were implemented, there was a reduction of 27.8% at 12.3 Hz in the axial direction and a reduction of 58.7% at 6.0 Hz in the tangential direction. This performance can likely be improved by combining both axes into a single H_∞ formulation. From these results, the H_∞ control design seems to be an effective tool for the control of reaction force vibration isolation systems.

REFERENCES

[1] Yuan, L., Pan, Z., Ding, D., Sun, S. and Li, W., 2018. A review on chatter in robotic machining process regarding both regenerative and mode coupling mechanism. *IEEE/ASME Transactions on mechatronics*, *23*(5), pp.2240-2251.

[2] Cvitanic, T., Nguyen, V. and Melkote, S.N., 2020. Pose optimization in robotic machining using static and dynamic stiffness models. *Robotics and Computer-Integrated Manufacturing*, *66*, p.101992.

[3] Nguyen, V., Cvitanic, T. and Melkote, S., 2019. Data-driven modeling of the modal properties of a six-degrees-of-freedom industrial robot and its application to robotic milling. *Journal of Manufacturing Science and Engineering*, *141*(12), p.121006.

[4] Kaldestad, K.B., Tyapin, I. and Hovland, G., 2015, July. Robotic face milling path correction and vibration reduction. In *2015 IEEE International Conference on Advanced Intelligent Mechatronics (AIM)* (pp. 543-548). IEEE.

[5] Yoshimura, T., Kume, A., Kurimoto, M. and Hino, J., 2001. Construction of an active suspension system of a quarter car model using the concept of sliding mode control. *Journal of Sound and Vibration*, *239*(2), pp.187-199.

[6] Kruczek, A. and Stribrsky, A., 2004, June. A full-car model for active suspension-some practical aspects. In *Proceedings of the IEEE International Conference on Mechatronics, 2004. ICM'04.* (pp. 41-45). IEEE.

[7] Kato, T., Kawashima, K., Funaki, T., Tadano, K. and Kagawa, T., 2010. A new, high precision, quick response pressure regulator for active control of pneumatic vibration isolation tables. *Precision Engineering*, *34*(1), pp.43-48.

[8] Guo, Y., Dong, H., Wang, G. and Ke, Y., 2016. Vibration analysis and suppression in robotic boring process. *International Journal of Machine Tools and Manufacture*, *101*, pp.102-110.

[9] Nguyen, V., Johnson, J. and Melkote, S., 2020. Active vibration suppression in robotic milling using optimal control. *International Journal of Machine Tools and Manufacture*, *152*, p.103541.

[10] Zimmerman, D.C. and Inman, D.J., 1990. On the nature of the interaction between structures and proof-mass actuators. *Journal of guidance, control, and dynamics*, *13*(1), pp.82-88.

[11] Auckly, D., Kapitanski, L. and White, W., 2000. Control of nonlinear underactuated systems. *Communications on Pure and Applied Mathematics: A Journal Issued by the Courant Institute of Mathematical Sciences*, *53*(3), pp.354-369.

[12] Xu, R. and Özgüner, Ü., 2008. Sliding mode control of a class of underactuated systems. *Automatica*, *44*(1), pp.233-241.

[13] Zames, G., 1981. Feedback and optimal sensitivity: Model reference transformations, multiplicative seminorms, and approximate inverses. *IEEE Transactions on automatic control*, *26*(2), pp.301-320.

[14] Huo, L., Song, G., Li, H. and Grigoriadis, K., 2007. Robust control design of active structural vibration suppression using an active mass damper. *Smart materials and structures*, *17*(1), p.015021.

SECTION

2. CONCLUSIONS AND RECOMMENDATIONS

Addressing the accuracy issue in robotics is paramount for improving their machining capabilities. In terms of positioning accuracy, there has been a plethora of research in the field of constructing more sophisticated kinematic models, but there has been a lack of research into rigously evaluating such models. When evaluating kinematic models, it is impossible to validate the model due to the potential of unmeasured "bad" locations, but it is possible to invalidate a model. When invalidating a model, it is important to consider the stochastic errors in the measurements as ignoring them can cause rejections of good kinematic models. A Model Invalidation method was proposed using a hypothesis testing framework combined with a sampling strategy that describes whether to explore new joint configurations or re-visit previous locations with large error. This methodology was shown to have an improved assessment of model accuracy over intuitive methods that are traditionally used.

When considering chatter in robotic machining, vibrations are typically due to mode-coupling chatter, which occur due to deflections of the robot arm itself and thus appear at low frequencies near the robot's first vibrational mode. To suppress these vibrations, a reaction force methodology was used which oscillates a mass back and forth opposite of the robot's vibrations in order to dampen the motion at the robot's first mode. This was accomplished by using an H_∞ control structure that utilized the frequency response of the robot as well as weighting functions on the robot's acceleration, the

reaction mass's position, and the control signal to generate a control algorithm. This controller was then implemented on an experimental robotic machining system for both single-axis and two-axis vibration suppression. In both tests, the vibration suppression system was shown to reduce robot accelerations at its first vibrational mode. This provides a framework for future vibration suppression as well as providing a basis for expansion to a full six degree of freedom vibration suppression.

From this work, two of the major issues in robotic machining were addressed. It is hoped that through these contributions the usage of robots in machining will expand, resulting in faster production, cheaper parts, and better working conditions.

VITA

Patrick Robert Thomas Bazzoli was raised in Beavercreek, Ohio. Patrick earned his Bachelor of Science in Mechanical Engineering from Missouri University of Science and Technology in 2014. In May 2024, he received his Ph.D. in Mechanical Engineering from Missouri University of Science and Technology.